

Magneto-elastic excitations in spin-Peierls systems

Michael Holicki* and Holger Fehske

Physics Department, University of Bayreuth, D-95440 Bayreuth, Germany

Ralph Werner

Physics Department, University of Wuppertal, D-42097 Wuppertal, Germany, and

Physics Department, Brookhaven National Laboratory, Upton, NY 11973-5000

(October 25, 2018)

Preprint. Typeset using REVTeX

Within the random phase approximation to the spin-Peierls transition two parameter regimes of phonon softening and hardening are present. Magneto-elastic excitations are discussed in detail for phonons coupled to the exactly solvable model of XY spin chains for both regimes, leading to a modified interpretation of the 30 cm^{-1} mode in CuGeO_3 . Frustrated Heisenberg chains coupled to phonons satisfactorily describe the pre-transitional quasi-elastic scattering in CuGeO_3 . A real space interpretation of the quasi-elastic scattering is given justifying effective Ising model approaches.

I. INTRODUCTION

The combined approach of the random-phase-approximation (RPA) for the spin-phonon coupling and bosonization for the spin dynamics applied by Cross and Fisher¹ to describe the spin Peierls-transition is consistent not only with the phonon softening in materials as TTCuBDT as initially believed but also with the hardening of the Peierls-active phonon modes in CuGeO_3 .^{2,3} The applicability of RPA is supported by the good agreement of mean-field results with experiments⁴⁻⁶ and the Ginzburg criterion.⁵⁻⁷

In the parameter regime where phonon hardening occurs the RPA calculations predict the appearance of spectral weight in the center of the phonon spectrum ($\omega \sim 0$) as a precursor of the phase transition. The precursor has been observed experimentally in CuGeO_3 and its temperature dependent intensity in neutron^{8,9} and X-ray^{10,11} scattering experiments has been shown to be satisfactorily reproduced within RPA.¹² We discuss in this paper the details of the precursor such as its momentum space dependence,^{9,8,11} the extracted correlation lengths,⁹⁻¹¹ its frequency dependence, and its real-space interpretation.

The relevant magnetic correlation function in the RPA approach is the dynamic dimer-dimer correlation

function.^{1,2,13} The determination of dynamic correlation functions is not evident even for exactly solvable one-dimensional models.^{14,15} The XY model is an exception¹⁶ and since there are similarities to the Heisenberg model^{17,12} it is an appropriate model to derive qualitative results exactly. Our studies of the coupling of phonons to XY spin chains show that the quasi-elastic scattering is the precursor of a new magneto-elastic excitation appearing at the phase transition. In the regime of phonon softening the mixed magneto-elastic nature of the “soft phonon” also becomes apparent.

The spin-phonon coupled Hamiltonian $H = H_s + H_p + H_{sp}$ relevant for spin-Peierls systems has been derived explicitly for CuGeO_3 .⁵ It consists of three parts. One is the Heisenberg spin-chain Hamiltonian

$$H_s = J \sum_{\mathbf{l}} \mathbf{S}_{\mathbf{l}} \cdot \mathbf{S}_{\mathbf{l}+\hat{z}} + J_2 \sum_{\mathbf{l}} \mathbf{S}_{\mathbf{l}} \cdot \mathbf{S}_{\mathbf{l}+2\hat{z}} \quad (1)$$

with the superexchange integrals J and J_2 between nearest-neighbor (NN) and next-nearest-neighbor (NNN) Cu d orbitals, respectively, and spin $1/2$ operators $\mathbf{S}_{\mathbf{l}}$ at Cu site \mathbf{l} in the three-dimensional lattice. \hat{z} is a unit vector along the spin-chain direction. The harmonic phonon part

$$H_p = \sum_{\mathbf{q}, \nu} \hbar \Omega_{\nu, \mathbf{q}} \left(b_{\nu, \mathbf{q}}^\dagger b_{\nu, \mathbf{q}} + \frac{1}{2} \right) \quad (2)$$

contains the dispersions $\Omega_{\nu, \mathbf{q}}$ for the relevant phonon modes³ labeled $\nu \in \{1, 2, 3, 4\}$ and Bose operators $b_{\nu, \mathbf{q}}^\dagger$ and $b_{\nu, \mathbf{q}}$. The spin-phonon coupling term is given by

$$H_{sp} = \frac{1}{\sqrt{N}} \sum_{\mathbf{q}} Y_{-\mathbf{q}} \sum_{\nu} g_{\nu, \mathbf{q}} \left(b_{\nu, -\mathbf{q}}^\dagger + b_{\nu, \mathbf{q}} \right). \quad (3)$$

N is the number of unit cells in the lattice. The coupling constants $g_{\nu, \mathbf{q}}$ depend on the polarization vectors of phonon mode ν and the Fourier transformed dimer operator is defined as

$$Y_{-\mathbf{q}} := \sum_{\mathbf{l}} e^{i\mathbf{q}\mathbf{R}_{\mathbf{l}}} \mathbf{S}_{\mathbf{l}} \cdot \mathbf{S}_{\mathbf{l}+\hat{z}}. \quad (4)$$

To compare with neutron or X-ray scattering data the phonon dynamic structure factor $S(\mathbf{q}, \omega)$ has to be determined. It is given via the imaginary part of the retarded normal coordinate propagator $D_{\nu}^{\text{ret}}(\mathbf{q}, \omega)$

*Present address: Mathematisches Institut, Universität Leipzig, D-04109 Leipzig, Germany

$$S(\mathbf{q}, \omega) = -\frac{1}{\pi} \frac{\sum_{\nu} \text{Im} D_{\nu}^{\text{ret}}(\mathbf{q}, \omega)}{1 - \exp(-\beta \hbar \omega)}. \quad (5)$$

We introduced the inverse temperature $\beta = 1/(k_B T)$. The retarded normal coordinate propagator is obtained through analytical continuation of the Matsubara propagator onto the real frequency axis

$$D_{\nu}^{\text{ret}}(\mathbf{q}, \omega) = \lim_{\epsilon \rightarrow 0} D_{\nu}(\mathbf{q}, i\omega_n \rightarrow \hbar\omega + i\epsilon), \quad (6)$$

where the latter is given in RPA¹³ by

$$D_{\nu}(\mathbf{q}, i\omega_n) = D_{\nu}^{(0)}(\mathbf{q}, i\omega_n) \times \frac{1 - \chi(\mathbf{q}, i\omega_n) \sum_{\nu' \neq \nu} g_{\nu', \mathbf{q}} g_{\nu', -\mathbf{q}} D_{\nu'}^{(0)}(\mathbf{q}, i\omega_n)}{1 - \chi(\mathbf{q}, i\omega_n) \sum_{\nu'} g_{\nu', \mathbf{q}} g_{\nu', -\mathbf{q}} D_{\nu'}^{(0)}(\mathbf{q}, i\omega_n)} \quad (7)$$

with bosonic Matsubara frequencies $\omega_n = 2\pi n/\beta$. The unperturbed propagator is

$$D_{\nu}^{(0)}(\mathbf{q}, i\omega_n) = -\frac{2 \hbar \Omega_{\nu, \mathbf{q}}}{\omega_n^2 + \hbar^2 \Omega_{\nu, \mathbf{q}}^2}. \quad (8)$$

The dimer-dimer correlation function

$$\chi(q_z, i\omega_n) = -\frac{1}{N} \int_0^{\beta} d\tau e^{i\omega_n \tau} \langle Y_{\mathbf{q}}(\tau) Y_{-\mathbf{q}}(0) \rangle \quad (9)$$

depends only on momenta q_z along the spin chains. Since the exact determination of $\chi(q_z, i\omega_n)$ in the case of the Heisenberg model is impossible we first study the case of the XY model. In Sec. III we then turn to the application of the RPA results on CuGeO₃, where a combination of analytical and numerical results is used to determine the dimer-dimer correlation function as accurate as possible.

II. MAGNETOSTRICTIVE XY MODEL

It is commonly accepted that the basic features of the spin-Peierls transition are well described by a one-dimensional spin model coupled magneto-elastically to the three-dimensional phonon system. The neglect of magnetic inter-chain coupling and frustration effects is certainly justified if the spin-phonon interaction dominates these spin interactions and causes the dimerization. Concerning the spin system, Caron and Moukouri¹⁸ showed that the simple XY spin chain model with $J_2 = 0$,

$$H_s = J \sum_{l \equiv l_z=1}^N (S_l^x S_{l+1}^x + S_l^y S_{l+1}^y), \quad (10)$$

contains the relevant physics of a spin-Peierls system, mainly because its excitation spectrum exhibits the requisite degeneracy with the ground state.¹⁹ In general, the mixed dimensionality of magnetic and spin-phonon interactions makes a theoretical treatment difficult. However, within the RPA (mean-field) approach in the spin-phonon coupling results obtained for a purely 1D phonon

system will be the same as those for a 3D phonon system,²⁰ whose polarization vectors satisfy $\mathbf{e}_{\nu, q_z} \cdot \hat{z} = \delta_{\nu, 1}$ and whose dispersion along the chain is

$$\Omega_q^2 \equiv \Omega_{1, q, \hat{z}}^2 = \frac{1}{2} \Omega_{\pi}^2 [1 - \cos(q)], \quad (11)$$

i.e., only one acoustic phonon branch couples to the magnetic system. In Eq. (11), the longitudinal wave number $q = q_z$ is given in units of the reciprocal lattice spacing $1/c$.

A. Uniform Phase

In solving the magnetostrictive XY model it is convenient to transform the spin-operators (S^x, S^y) to operators of spinless fermions ($d_l^{(\dagger)}$), via the Jordan-Wigner transformation.²¹ Then, in the uniform phase above T_{SP} , we start from the following (Fourier transformed) Hamiltonian

$$H = H_p + H_s + H_{sp} = \sum_q \Omega_q b_q^{\dagger} b_q + \sum_k E_k d_k^{\dagger} d_k + \frac{1}{\sqrt{N}} \sum_q g_q Y_{-q} (b_q + b_{-q}^{\dagger}) \quad (12)$$

with

$$E_k = \cos(k), \quad (13)$$

$$g_q = \left(\frac{\lambda \Omega_{\pi}^2 \pi}{\Omega_q} \right)^{\frac{1}{2}} (1 - e^{iq}), \quad (14)$$

$$\lambda = \frac{g^2}{2\pi m \Omega_{\pi}^2}, \quad g = \left. \frac{dJ}{dr} \right|_{r=c}, \quad (15)$$

and $q, k \in]-\pi, \pi]$ (in this section, we drop the factors \hbar, k_B and define all energies in units of J). The dimer operator (4) is now

$$Y_{-q} = \sum_l e^{iql} (S_l^x S_{l+1}^x + S_l^y S_{l+1}^y) = \frac{1}{2} \sum_k (e^{i(k-q)} + e^{-ik}) d_k^{\dagger} d_{k-q}. \quad (16)$$

Inserting Eq. (11) we see that the ground-state and thermodynamic properties of the model (12) are governed by two independent control parameters: (i) the dimensionless coupling constant λ and (ii) the ratio of phononic to magnetic energy scale Ω_{π} . λ is independent of the ion mass m because $\Omega_{\pi}^2 \sim 1/m$. It will turn out that the transition temperature and the static dimerization is a function of λ alone. For a constant λ , Ω_{π} is a measure for the mass of the ions; small values of Ω_{π} describe the adiabatic, large values the anti-adiabatic regime.

For the model (12), the RPA Matsubara Green's function (7) becomes

$$D(q, i\omega_n) = D^{(0)}(q, i\omega_n) \frac{1}{1 - D^{(0)}(q, i\omega_n)P(q, i\omega_n)}, \quad (17)$$

where the self energy is defined as

$$P(q, i\omega_n) = g_q g_{-q} \chi(q, i\omega_n). \quad (18)$$

The dimer-dimer correlation function (9) is

$$\chi(q, i\omega_n) = \frac{1}{4\pi} \int_{-\pi}^{\pi} dk (1 + \cos(2k + q)) K_{k,q}(i\omega_n), \quad (19)$$

with the Lindhard kernel

$$K_{k,q}(i\omega_n) = \frac{f_{k+q} - f_k}{i\omega_n + E_{k+q} - E_k}, \quad (20)$$

where $f_k = 1/(e^{\beta E_k} + 1)$ is the Fermi distribution function.

Having calculated the Matsubara propagator we can easily obtain the retarded Green's function on the real frequency axis according to Eq. (6). A structural instability is always connected to a pole of $D^{\text{ret}}(q, \omega)$ at $\omega = 0$, leading to a spontaneous transition to a broken-symmetry ground state at $T = 0$. At finite temperature, the instability condition for a lattice distortion with wave number q is

$$\frac{1}{2\lambda} = \int_{-\pi}^{\pi} dk (1 + \cos(2k + q)) K_{k,q}(0), \quad (21)$$

which is the same result as derived by Lima and Tsallis²² in the adiabatic limit ($m \rightarrow \infty$). It turns out that the π mode is the first (and only) one that gets unstable. Therefore the lattice will dimerize below a transition temperature T_{SP} , which can be obtained from the numerical solution of Eq. (21) at $q = \pi$. The inverse transition temperature is shown in Fig. 1 together with the results obtained from high and low temperature expansions,

$$\beta_{\text{SP}} = \frac{1}{\lambda\pi} \quad \lambda \gg 1, \quad (22)$$

$$\beta_{\text{SP}} = 1.19 \cdot \exp\left(\frac{1}{8\lambda}\right) \quad \lambda \ll 1, \quad (23)$$

respectively.

B. Dimerized Phase

Below the transition temperature T_{SP} the systems is in a less-symmetric but lower energy configuration. The lattice is dimerized which causes the unit cell to double in size, which in reciprocal space means that $q, k \in]-\pi/2, \pi/2]$. To include a static dimerization δ in our Hamiltonian explicitly, we perform a unitary transformation

$$\tilde{H} = e^S H e^{-S}, \quad (24)$$

with

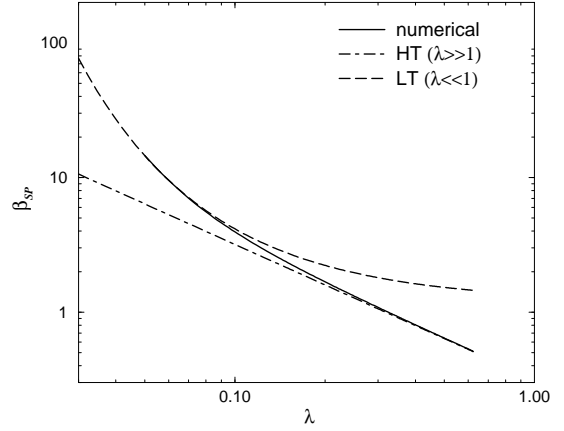


FIG. 1. Inverse spin-Peierls transition temperature β_{SP} vs. coupling constant λ (solid line). The dot-dashed (dashed) curve denotes the high (low) temperature approximation.

$$S = \frac{1}{4} \sqrt{\frac{N}{\pi \Omega_\pi}} \delta(b_\pi - b_\pi^\dagger). \quad (25)$$

In a next step, we redefine the Fourier transformed fermion operators²³

$$c_k = \sqrt{\frac{2}{N}} \sum_{l=1}^{\frac{N}{2}} e^{-i(2l-1)k} d_{2l-1}, \quad (26)$$

$$\bar{c}_k = \sqrt{\frac{2}{N}} \sum_{l=1}^{\frac{N}{2}} e^{-i(2l)k} d_{2l}, \quad (27)$$

and remove the non-diagonal c - \bar{c} cross-terms by a canonical Bogoliubov transformation

$$c_k = \frac{1}{\sqrt{2}}(\gamma_k + \beta_k), \quad \bar{c}_k = \frac{1}{\sqrt{2}}(\gamma_k - \beta_k)e^{i\Theta_k}, \quad (28)$$

where

$$\Theta_k = \arctan\left(\sqrt{\lambda}\delta\right). \quad (29)$$

For the phonon part, we now have two modes denoted by ν , an acoustical ($\nu = 0$) and an optical ($\nu = 1$), where in the reduced Brillouin zone the phonon operators are

$$b_{\nu,q} = \begin{cases} b_{q+\nu\pi} & q \leq 0 \\ b_{q-\nu\pi} & q > 0, \end{cases} \quad (30)$$

and the dispersion is

$$\Omega_{\nu,q} = \Omega_{q+\nu\pi}. \quad (31)$$

Finally the Hamiltonian describing the dimerized phase takes the form

$$\tilde{H} = H_p + H_s + H_{dp} + H_{\text{elast}} + H_{sp}$$

$$\begin{aligned}
&= \sum_{q,\nu} \Omega_{\nu,q} b_{\nu,q}^\dagger b_{\nu,q} + \sum_k E_k (\gamma_k^\dagger \gamma_k - \beta_k^\dagger \beta_k) \\
&\quad - \delta \sqrt{\frac{N\Omega_\pi}{16\pi}} (b_{1,0} + b_{1,0}^\dagger) + \frac{N\delta^2}{16\pi} \\
&\quad + \frac{1}{\sqrt{N}} \sum_{\nu,q} g_{\nu,q} (Y_{\nu,-q}^\beta - Y_{\nu,-q}^\gamma - Z_{\nu,-q}^{\gamma\beta} + Z_{\nu,-q}^{\beta\gamma}) \\
&\quad \times (b_{\nu,q} + b_{\nu,-q}^\dagger), \quad (32)
\end{aligned}$$

with the operators

$$Y_{\nu,-q}^\gamma = \sum_k \left((-1)^\nu e^{i(k-q)} + e^{-ik} \right) T_{k,\nu,q} \gamma_k^\dagger \gamma_{k-q}, \quad (33)$$

$$Z_{\nu,-q}^{\gamma\beta} = \sum_k \left((-1)^\nu e^{i(k-q)} + e^{-ik} \right) T_{k,\nu+1,q} \gamma_k^\dagger \beta_{k-q}, \quad (34)$$

and

$$g_{\nu,q} = \left(\frac{\lambda \Omega_\pi^2 \pi}{\Omega_{\nu,q}} \right)^{\frac{1}{2}} (1 - (-1)^\nu e^{iq}), \quad (35)$$

$$E_k = \sqrt{\cos^2(k) + \lambda \delta^2 \sin^2(k)} = E_k^\gamma = -E_k^\beta, \quad (36)$$

$$T_{k,\nu,q} = \frac{1}{4} (e^{i\Theta_{k-q}} + \alpha_{k-q} (-1)^\nu e^{-i\Theta_k}). \quad (37)$$

The phase factor α_{k-q} is 1 for normal ($|k-q| < \frac{\pi}{2}$) and -1 for Umklapp ($|k-q| > \frac{\pi}{2}$) processes. Accordingly, instead of one fermion band as in the uniform case, we now have two bands, separated by a gap proportional to δ . The operators Y and Z describe intra- and inter-band transitions, respectively (see Fig. 2).

The parameter δ is not yet defined. Due to the invariance of the trace under canonical transformations the following relation holds for all values of δ

$$\begin{aligned}
0 &= -\frac{\partial}{\partial \delta} \frac{1}{\beta} \ln \left(\text{Tr} e^{-\beta \tilde{H}} \right) \\
&= \sum_k \frac{\lambda \delta}{E_k} \langle \gamma_k^\dagger \gamma_k - \beta_k^\dagger \beta_k \rangle_{\tilde{H}} - \sqrt{\frac{N\Omega_\pi}{16\pi}} \langle b_{1,0} + b_{1,0}^\dagger \rangle_{\tilde{H}} \\
&\quad + \frac{N\delta}{8\pi} + \left\langle \frac{\partial}{\partial \delta} H_{sp} \right\rangle_{\tilde{H}}. \quad (38)
\end{aligned}$$

To determine δ , we demand that the phonon coordinates have expectation value zero with respect to \tilde{H} :

$$\langle b_{1,0} + b_{1,0}^\dagger \rangle_{\tilde{H}} \stackrel{!}{=} 0. \quad (39)$$

This means that we generated a Hamiltonian \tilde{H} with $q = 0$, $\nu = 1$ modes shifted by δ in a way that the expectation value of the b -operators under the new Hamiltonian is zero. Therefore δ is the equilibrium position of the π mode under the original Hamiltonian H (the static dimerization):

$$\delta \propto \langle b_\pi + b_\pi^\dagger \rangle_H. \quad (40)$$

If the calculations are not done in Fourier but in real space, it can easily be shown²⁴ that the δ determined by

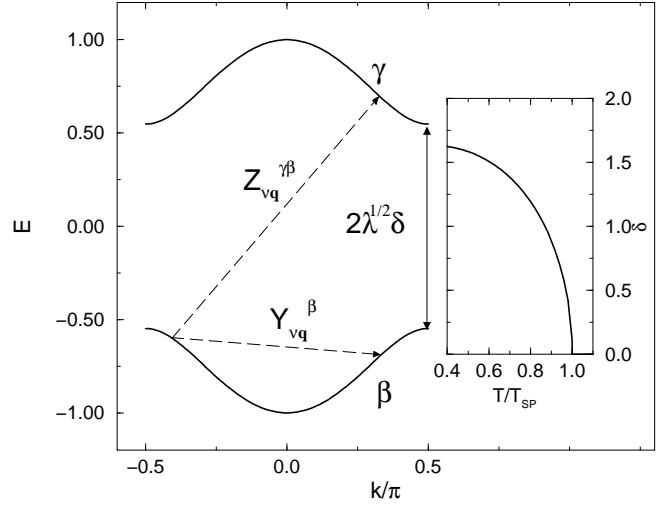


FIG. 2. Fermion band structure in the dimerized phase (left panel). The dashed arrows indicate the processes described by the Y and Z operators. The right panel shows the temperature dependence of the dimerization δ for $\lambda = 0.1$.

this prescription is directly proportional to the magnetic order parameter used by other authors²⁵:

$$\delta \propto \left\langle \frac{1}{N} \sum_l (-1)^l (S_l^x S_{l+1}^x + S_l^y S_{l+1}^y) \right\rangle_{\tilde{H}}. \quad (41)$$

From Eq. (38), besides the trivial solution $\delta = 0$, finite- δ solutions can be obtained from the gap equation,

$$1 = 4\lambda \int_{-\frac{\pi}{2}}^{\frac{\pi}{2}} \frac{\tanh\left(\frac{\beta E_k}{2}\right)}{E_k} \sin^2(k) dk, \quad (42)$$

which show the typical behavior of an order parameter for a second-order phase transition (cf. inset of Fig. 2).

As the Y and Z operators depend on the phonon band index ν , Eq. (7) for the phonon Green's function must be modified. An additional term $C(q, i\omega_n)$ in the denominator appears. The RPA propagator becomes

$$\begin{aligned}
D_\nu(q, i\omega_n) &= D_\nu^{(0)}(q, i\omega_n) \\
&\quad \times \frac{1 - \sum_{\mu \neq \nu} P_\mu(q, i\omega_n) D_\mu^{(0)}(q, i\omega_n)}{1 - \sum_\mu P_\mu(q, i\omega_n) D_\mu^{(0)}(q, i\omega_n) + C(q, i\omega_n)}, \quad (43)
\end{aligned}$$

with

$$\begin{aligned}
C(q, i\omega_n) &= D_0^{(0)}(q, i\omega_n) D_1^{(0)}(q, i\omega_n) \\
&\quad \times (P_1(q, i\omega_n) P_0(q, i\omega_n) - Q_1(q, i\omega_n) Q_0(q, i\omega_n)), \quad (44)
\end{aligned}$$

$$\begin{aligned}
P_\nu(q, i\omega_n) &= g_{\nu,-q} g_{\nu,q} \left(\chi_\nu^\gamma(q, i\omega_n) + \chi_\nu^\beta(q, i\omega_n) \right. \\
&\quad \left. + \zeta_\nu^{\beta\gamma}(q, i\omega_n) + \zeta_\nu^{\gamma\beta}(q, i\omega_n) \right), \quad (45)
\end{aligned}$$

$$Q_\nu(q, i\omega_n) = g_{\nu,-q} g_{|1-\nu|,q} \left(\hat{\chi}^\gamma(q, i\omega_n) + \hat{\chi}^\beta(q, i\omega_n) + \hat{\zeta}^{\beta\gamma}(q, i\omega_n) + \hat{\zeta}^{\gamma\beta}(q, i\omega_n) \right). \quad (46)$$

Here

$$\chi_\nu^\gamma(q, i\omega_n) = \int_{-\frac{\pi}{2}}^{\frac{\pi}{2}} \frac{dk}{4\pi} (1 + \alpha_{k+q}(-1)^\nu \cos(\Theta_k + \Theta_{k+q})) \times (1 + (-1)^\nu \cos(2k + q)) K_{k,q}^{\gamma\gamma}(i\omega_n), \quad (47)$$

$$\hat{\chi}^\gamma(q, i\omega_n) = - \int_{-\frac{\pi}{2}}^{\frac{\pi}{2}} \frac{dk}{4\pi} \sin(\Theta_k + \Theta_{k+q}) \alpha_{k+q} \times \sin(2k + q) K_{k,q}^{\gamma\gamma}(i\omega_n) \quad (48)$$

denote Y-Y (intra-band) and

$$\zeta_\nu^{\gamma\beta}(q, i\omega_n) = \int_{-\frac{\pi}{2}}^{\frac{\pi}{2}} \frac{dk}{4\pi} (1 - \alpha_{k+q}(-1)^\nu \cos(\Theta_k + \Theta_{k+q})) \times (1 + (-1)^\nu \cos(2k + q)) K_{k,q}^{\gamma\beta}(i\omega_n), \quad (49)$$

$$\hat{\zeta}^{\gamma\beta}(q, i\omega_n) = - \int_{-\frac{\pi}{2}}^{\frac{\pi}{2}} \frac{dk}{4\pi} \sin(\Theta_k + \Theta_{k+q}) \alpha_{k+q} \times \sin(2k + q) K_{k,q}^{\gamma\beta}(i\omega_n), \quad (50)$$

Z-Z (inter-band) correlation functions, respectively, both depending on a generalized Lindhard kernel

$$K_{k,q}^{\gamma\beta}(i\omega_n) = \frac{f_{k+q}^\gamma - f_k^\beta}{i\omega_n + E_{k+q}^\gamma - E_k^\beta}. \quad (51)$$

Note that Eq. (43) simplifies substantially for the $q = 0$, $\nu = 1$ mode, as for $\omega_n \neq 0$, $q \rightarrow 0$ all terms containing $D_0^{(0)}(q, i\omega_n)$ vanish.

C. Numerical Results

The mechanism driving the spin-Peierls phase transition is best understood by examining the phonon dynamical structure factor. Here we concentrate on the unstable π mode (which is folded back to the $q = 0$, $\nu = 1$ mode in the reduced Brillouin zone). When we calculate $S(\pi, \omega)$ for an interacting electron- (spin-) phonon system, we typically find a broad distribution of spectral weight. It is clear that a phonon can only be absorbed by the fermion system, if its energy and momentum equal the ones of a fermionic excitation. Therefore, in the uniform phase for $q = \pi$ we found a band of damped excitations for $\omega < 2$. In the dimerized phase, there is a gap in the electronic spectrum (cf. Fig. 2), so damped excitations exist only in the energy interval $2\sqrt{\lambda}\delta < \omega < 2$. On the other hand, sharp peaks in the structure factor correspond either to those (bare) phonon modes which are outside the fermionic band and thus excluded from scattering processes by energy conservation or to *new* quasi-particle excitations of the coupled spin-phonon system.

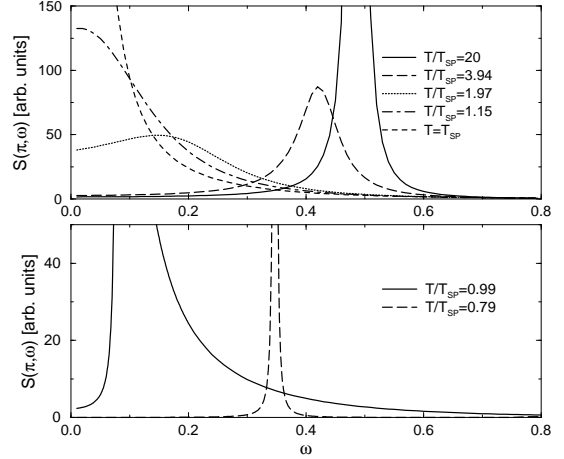


FIG. 3. Dynamical structure factor $S(\pi, \omega)$ in the soft mode regime ($\Omega_\pi = 0.5$, $\lambda = 0.1$). In the uniform phase the high temperature peak softens until it reaches zero at $T = T_{\text{SP}}$ (upper panel). In the dimerized phase it gets harder again (lower panel).

In the high temperature limit ($T \rightarrow \infty$), the correlation function $\chi(\pi, \omega)$ vanishes. Therefore we get a sharp peak at $\omega = \Omega_\pi$ corresponding to the non-interacting phonon. As the temperature is lowered two distinct regimes appear, depending on the frequency of the π phonon. For low values of Ω_π , i.e., in the *adiabatic regime*, the high temperature peak moves towards lower energies and substantially broadens, until it reaches zero, where it stays and gets larger in magnitude until a divergence appears at $T = T_{\text{SP}}$ (Fig. 3). This is called a *soft mode scenario*. Below the transition, the peak moves towards higher energies. For large values of Ω_π , i.e., in the *anti-adiabatic regime* we found a completely different behavior, usually termed *central peak scenario*. Here the high temperature peak does not soften, it even gets harder. However, with lowering the temperature a maximum in $S(\pi, \omega)$ arises at $\omega = 0$, related to quasi-elastic scattering processes. The height of this peak structure increases with decreasing temperature until it diverges at $T = T_{\text{SP}}$, where $S(\pi, \omega) \propto \omega^{-2}$ (Fig. 4). For $T < T_{\text{SP}}$ the structure factor consists of three parts: a delta peak slightly above Ω_π which can be attributed to the original π -phonon mode, the scattering continuum in the range $2\sqrt{\lambda}\delta < \omega < 2$ and a pronounced peak below the continuum, which is the central peak that moved from $\omega = 0$ to higher energies. Let us point out that the magnetostrictive Heisenberg model shows the same qualitative behavior. This model will be studied in more detail in Sec. III, also in relation to the experimental findings for GuGeO_3 at $T > T_{\text{SP}}$.

Here we complete our study of the magnetostrictive XY model by examining the pole structure of the retarded propagator (for $q = \pi$) in the whole complex ω -plane. The prescription (6) can easily be generalized for a complex ω in the upper half plane. In the lower complex plane, however, we are faced with the prob-

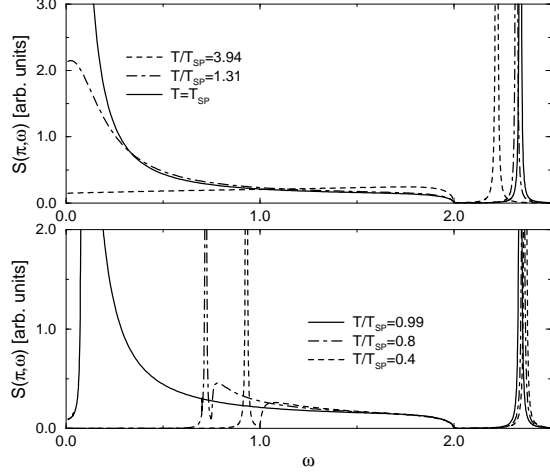


FIG. 4. Dynamical structure factor $S(\pi, \omega)$ in the central peak regime ($\Omega_\pi = 2.1$, $\lambda = 0.1$). The high temperature peak does not soften, it even gets slightly harder. A peak at $\omega = 0$ appears in the uniform phase that becomes a singularity at $T = T_{SP}$ (upper panel). In the dimerized phase, it moves towards higher energies, corresponding to a second excitation (lower panel).

lem that $\chi(q, \omega)$ has a branch cut on the real axis at $\omega \in [-2; 2]$ (in the uniform phase). This means that there are two possibilities to continue D^{ret} analytically to the lower half plane, i.e., there exist two branches. The first branch is analytical everywhere on the complex plane, except at $\omega \in [-2; 2]$, the second everywhere except $\omega \in]-\infty; -2] \cup [2; \infty[$. They are both of course identical in the upper half plane. The first branch is directly obtained by evaluating the integral in Eq. (19) for an ω with $\text{Im}\omega < 0$. We get the second by extrapolation from the upper half plane for $\text{Re}\omega \in [-2; 2]$ (this is done by a fourth order power series). It turns out that the first branch will yield purely real poles with $\text{Re}\omega > 2$, the second branch corresponds to poles with negative imaginary part and $\text{Re}\omega < 2$.

When lowering the temperature in the *soft mode regime* (see Fig. 5) the real part of the high temperature pole decreases from Ω_π to 0 at a temperature larger than T_{SP} . The modulus of the imaginary part grows with decreasing temperatures and reaches a maximum at the temperature where the real part gets to zero for the first time. Then it decreases again. At $T = T_{SP}$ we have $\omega = 0$ as expected. For lower temperatures the pole is real and its value increases until it saturates at $T = 0$. In the *central peak regime* (see Fig. 6) the high temperature pole ω_1 gets harder. A second pole ω_2 , which is purely imaginary for $T > T_{SP}$ appears and causes the instability at $T = T_{SP}$. For $T < T_{SP}$ this pole is real and increasing as $T \rightarrow 0$.

Although the interpretation of real and imaginary part of a complex singularity as energy and damping of a quasiparticle is doubtful in the presence of a branch cut,²⁶

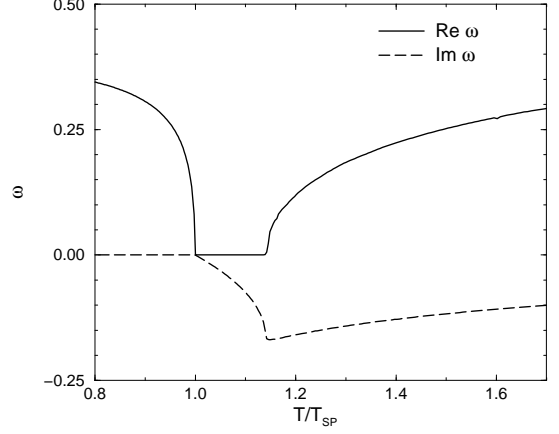


FIG. 5. Real and imaginary part of the pole of the retarded Green's function in the soft mode regime ($\Omega_\pi = 0.5$, $\lambda = 0.1$).

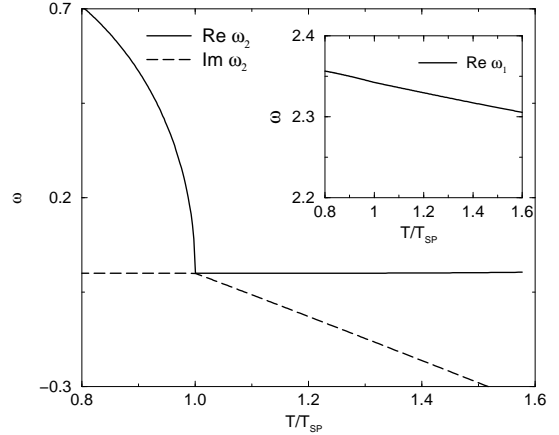


FIG. 6. Poles of the retarded Green's function in the central peak regime ($\Omega_\pi = 2.1$, $\lambda = 0.1$). The (real) high temperature pole ω_1 does not soften, as shown in the inset. Instead a second pole ω_2 appears, which is purely imaginary in the uniform phase and gets real in the dimerized phase.

examining the pole structure still gives a qualitative understanding of the mechanism driving the phase transition. Most notably, the purely imaginary structure factor just above T_{SP} signals quasi-elastic scattering, i.e. the existence of diffusive modes, in both the adiabatic and anti-adiabatic regimes. Of course, to get a complete picture, it is also necessary to take into account the spectral weight of the continuum seen in the structure factor.

D. Application to CuGeO_3

Even though the model we discussed is far too simple to expect a good quantitative description of CuGeO_3 it should at least produce effects in the right order of magnitude. To make contact with the experimentally observed magneto-elastic excitation spectrum of CuGeO_3 , in the

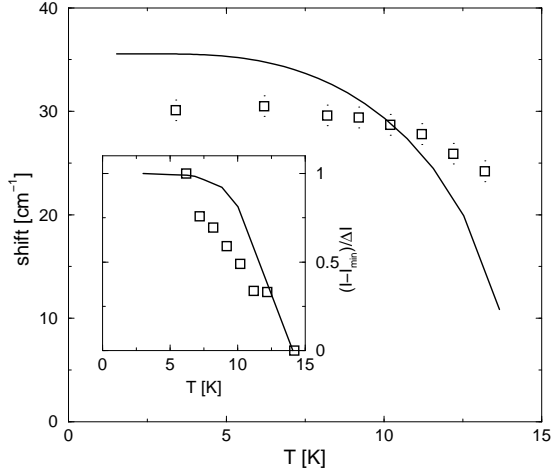


FIG. 7. Temperature dependence of the energy of the second magneto-elastic excitation obtained from the magnetostrictive XY model (solid line) compared to experimental data for the 30 cm^{-1} mode of CuGeO_3 (symbols)²⁷. The inset shows the rescaled spectral weight of this excitation vs. temperature (solid line) compared to experiment (symbols).²⁸

numerical calculations we fix the energy scale by $J = 150 \text{ K}$ and use $T_{\text{SP}} = 14 \text{ K}$ together with a phonon frequency of $\Omega_{\mathbf{q}_0}/2\pi = 6.53 \text{ THz}$ which corresponds to the dominant Peierls-active T_2^+ -phonon-mode.⁵ This gives the control parameters $\Omega_\pi = 2.09$ and $\lambda = 0.057$. For the spin gap at $T = 0$ we get $2\Delta = 2\sqrt{\lambda}\delta J = 4.422 \text{ meV}$ compared to an experimental value of $2\Delta = 4.2 \text{ meV}$.²⁷ The ground state exchange alternation is $\delta_J = \sqrt{\lambda}\delta = 0.1645$. Other methods give values from 0.01 to 0.2.⁵

As expected for CuGeO_3 , we are in the central peak regime. Thus we have a second excitation for $T \leq T_{\text{SP}}$. In recent inelastic light scattering (ILS) experiments a peak in the spectrum at 30 cm^{-1} was observed and interpreted as a singlet bound state of two antiparallel magnons.²⁷ One could now speculate that the excitation below scattering continuum we found in the structure factor is the phonon contribution of this new magneto-elastic excitation. A comparison of the theoretical and experimental²⁸ data for the position and intensity of this peak is given in Fig. 7. Theory and experiment show the same overall behavior, although the decrease of the peak position is much more pronounced in the theory.

Here the spin-phonon coupling gives rise to an effective spin-spin interaction²⁹ which, in the dimerized phase, leads to a *phonon-induced* bound state in the magnetic excitation spectrum just below the fermionic scattering continuum. A signature of this bound state appears in the phonon structure factor as shown in Fig. 4 proving its magneto-elastic character. In the case of dimerized Heisenberg chains the Jordan-Wigner transformation of the spin part gives directly a four-fermion interaction term¹⁶ leading to a peak in the dimer-dimer correlation function at $\sqrt{3}/2$ times the band gap.^{30,31} Due to the

phonon-induced effective spin-spin (fermion-fermion) interaction, the energy of this bound state will be shifted in the order of $\sum_\nu |g_{\nu, \mathbf{q}_0}|^2 / (\hbar \Omega_{\nu, \mathbf{q}_0}) \approx 0.1J$,¹³ which is a 10 % effect, and the bound state will appear in the phononic structure factor. This supports the interpretation of the peak at 30 cm^{-1} observed with inelastic light scattering as the singlet bound state as shown in Fig. 7. The quasi-elastic scattering is the precursor of this excitation. Moreover, the hardening of in the Peierls-active phonon modes observed in CuGeO_3 ³ is qualitatively well described within the RPA scheme,^{2,12} i.e., those initial elastic excitations also have a magnetic character.

To summarize, in this section we have performed a comprehensive study of the magnetostrictive XY model which is the minimal model capable of describing the spin-Peierls scenario in the whole phonon frequency range. The focus was on the anti-adiabatic central-peak regime being relevant for CuGeO_3 .

III. QUASI-ELASTIC SCATTERING IN CuGeO_3

In order to describe experimental results on CuGeO_3 accurately, the spin system to include are frustrated Heisenberg chains^{32–35} which is coupled to the four Peierls-active phonon modes. Frequencies and coupling constants of the Peierls-active T_2^+ phonons are discussed in detail in Refs. 3 and 5. The CuGeO_3 samples used for comparison with experiment in this section undergo the spin-Peierls transition at $T = 14.3 \text{ K}$, the theoretical calculations are adapted to match via the coupling constants. The wave vector of the modulation in the ordered phase is $\mathbf{q}_0 = (\pi/a, 0, \pi/c)$, where a and c are the lattice constant along the crystallographic x and z direction, respectively. We set $J/k_B = 150 \text{ K}$, which is together with a value of $J_2/J = 0.24$ among those discussed as valid for CuGeO_3 .^{5,36} Quasi-elastic scattering has been observed in neutron scattering experiments^{9,8} up to 16 K and in X-ray scattering¹⁰ up to 40 K or $k_B T \approx 0.3J$. The constants k_B and \hbar are explicitly given in this section for a more transparent unit conversion.

The dimer-dimer correlation function as given in Eq. (9) has been calculated for Heisenberg chains in the uniform phase by Cross and Fisher¹ with bosonization techniques. In the analytically continued form one has

$$\chi_{\text{CF}}(q_z, \omega) = \frac{-\chi_0(\frac{k_B T}{J})}{0.35 k_B T} I_1 \left[\frac{\omega - v_s |q_z - \frac{\pi}{c}|}{2\pi(k_B/\hbar)T} \right] I_1 \left[\frac{\omega + v_s |q_z - \frac{\pi}{c}|}{2\pi(k_B/\hbar)T} \right] \quad (52)$$

with the spin-wave velocity³⁷ $v_s = c(J - 1.12J_2)/(\pi\hbar)$ and the functions $I_1(k) = (8\pi)^{-1/2} \Gamma(\frac{1}{4} - \frac{1}{2}ik) \Gamma^{-1}(\frac{3}{4} - \frac{1}{2}ik)$. The result has the general form of spin correlation functions obtained from conformal field theory.^{38–40} The choice of the value of $J_2 = 0.24J \leq J_c$ allows for the application of the field-theoretical results. For $J_2 > J_c$ the spectrum of the spin system is gaped.⁴¹

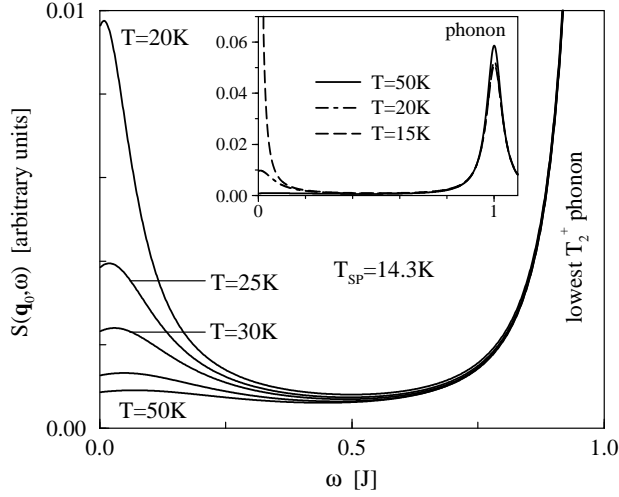


FIG. 8. Frequency dependence of the structure factor from Eq. (5) appropriate for CuGeO_3 . As the temperature approaches the spin-Peierls transition quasi-elastic scattering appears. Inset: larger scale representation. The phonon is the lowest of the four Peierls-active modes, see Refs. 3,5.

The prefactor $\chi_0(k_B T/J)$ is assumed constant in field theory but has been shown by Raupach *et al.* using density matrix renormalization group (DMRG) studies to be temperature dependent in the static case and for $q_z = \pi/c$.⁴² Recent numerical studies suggest that the approximate result Eq. (52) describes the exact dimer-dimer correlation function better when rescaling the energy as $\chi(q_z, \omega) = \chi_{\text{CF}}(q_z, g_T \omega)$, where the scaling function g_T depends on the NNN coupling J_2 . We use in this work the g_T as given in Ref. 12 for $J_2/J = 0.24$. Please note that none of the results presented herein depend qualitatively on the inclusion of g_T .

A. Frequency dependence

The frequency dependence of the dynamical structure factor Eq. (5) for the parameters relevant for CuGeO_3 is shown in Fig. 8. Below $T \sim 3T_{\text{SP}}$ spectral weight appears in the center of the spectrum. Expanding the complex $\chi_{\text{CF}}(\pi/c, \omega)$ to second order¹³ in ω in Eq. (7), the dynamical structure factor can be determined for $\hbar\omega \ll k_B T_{\text{SP}}$ to diverge as $S(\mathbf{q}_0, \omega)|_{T=T_{\text{SP}}} \sim \omega^{-2}$ at the phase transition.

By analogy to the XY model discussed in the previous section (compare Figs. 4, 6, and Sec. IID) this is the precursor of the magneto-elastic mode appearing at the phase transition. The Peierls-active phonons (only the lowest is shown in Fig. 8) harden as the temperature is lowered and the temperature dependence of the intensity of the quasi-elastic scattering is consistent with neutron and X-ray-scattering experiments.¹²

B. Momentum dependence

The momentum dependent scattering rate of inelastic neutrons or X-rays can be obtained by convoluting the dynamical structure factor Eq. (5) with a Gaussian of the width of the experimental energy resolution σ_ω and a Gaussian of the width of the experimental momentum resolution σ_{q_z} . The limitation to the chain direction is imposed since the dimer-dimer correlation function Eq. (52) only introduces a z axis dispersion:

$$I(q_z, \omega) = \frac{1}{2\pi\sigma_\omega\sigma_{q_z}} \int_{-\infty}^{\infty} d\omega' e^{-\frac{(\omega'-\omega)^2}{2\sigma_\omega^2}} \int_{1.\text{BZ}} d^3q e^{-\frac{(q'_z-q_z)^2}{2\sigma_{q_z}^2}} \times \delta(q_x - \pi/a) \delta(q_y) S(\mathbf{q}', \omega'). \quad (53)$$

The first Brillouin zone (1.BZ) is that in the disordered high temperature phase.

Fig. 9 shows plots of $I(q_z, 0)$ for different temperatures in comparison with neutron scattering data from Ref. 8. Parameters are chosen appropriate for CuGeO_3 as discussed above, the resolutions are $\hbar\sigma_\omega \approx 0.05J$ and $\sigma_{q_z} \approx 0.06/c$. The value of σ_ω is given by the experimental setup,² σ_{q_z} is obtained from the resolution limited Bragg peak at 4 K.⁸ The agreement with experiment is satisfactory. Note that the critical region has been estimated via the Ginzburg criterion⁵ to be $T_{\text{SP}} \pm 0.4$ K. Within this region the theoretical divergence of the intensity¹² is suppressed by critical fluctuations.

The experimental scans run along $[\pi/a(1+2p), \pi/b(8-2p), \pi/c(1+2p)]$. p is the running parameter, $q_y = 8\pi/b$ assures that there is no significant magnetic contribution to the signal.⁸ Since $c < a < b$ and since the correlations along q_z are clearly dominant,^{9,10} the data are still eligible for comparison with the theoretical data along q_z .

C. Correlation length

When correcting the momentum dependent quasi-elastic scattering shown in Fig. 9 for experimental resolution the data can be fitted nicely by Lorentzians.^{9,11} For $T - T_{\text{SP}} \leq 0.1$ K a second length scale appears which can be fitted by an additional Lorentzian squared contribution. It is attributed to surface strain effects^{11,43} not included in the RPA treatment.

From the width of the fits the correlation length can be extracted. The corresponding theoretical correlation length is obtained accordingly from Eq. (53) setting $\sigma_{q_z} = 0$. Figure 10 shows the importance of the energy resolution when discussing the temperature dependence of the extracted correlation length. The symbols mark the experimental data, open squares are from X-ray data in Ref. 10, full circles are neutron data in Ref. 9. The neutron data are shifted by $\Delta T = 1$ K in order to match the different critical temperatures of the samples.

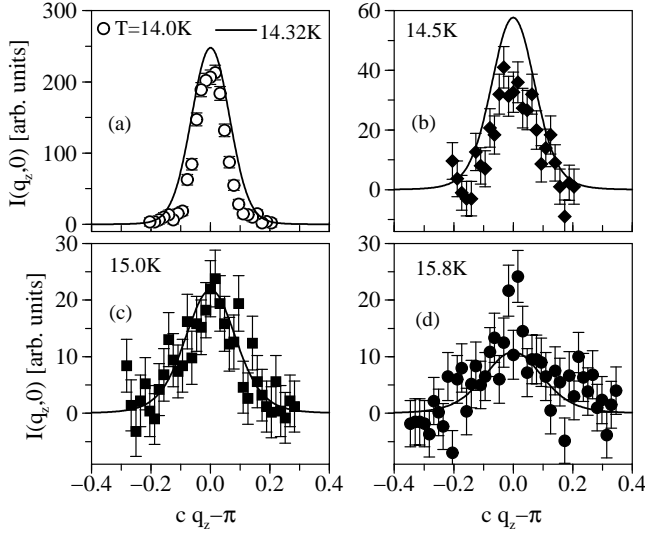


FIG. 9. Quasi-elastic scattering from neutrons (symbols, background subtracted, scaled with a unique factor for all temperatures) compared with theory from Eq. (53) (full lines) for different temperatures. (a) Due to critical fluctuations the experimental intensity does not diverge at the transition and reaches the value of the theoretical results only somewhat below the transition. In (b) temperature is still in the critical region, (c) and (d) show excellent agreement. The experimental scans run along $[\pi/a(1+2p), \pi/b(8-2p), \pi/c(1+2p)]$, see Sec. III B.

The energy resolution in neutron scattering is of the order of a few meV while X-rays integrate over a much larger energy interval. $\hbar\sigma_\omega \approx 0.05J$ simulates the resolution of diffracted neutrons² and $\hbar\sigma_\omega \approx 0.5J$ is relevant for X-ray scattering. The X-ray resolution is probably even larger, but the interval of $-0.5J < \hbar\omega < 0.5J$ covers the full width of the relevant magnetic spectrum.¹²

The following conclusions can be drawn from the results presented:

(i) The energy integration in X-ray scattering allows for the determination of the correlation to much higher temperatures than neutron scattering.¹²

(ii) The momentum and frequency dependence of $S(\mathbf{q}, \omega)$ cannot be factorized yielding the different magnitude of the theoretical results for $\hbar\sigma_\omega = 0.05J$ and $\hbar\sigma_\omega = 0.5J$, shown by the full lines in Fig. 10 (a) and (b), respectively.

(iii) The large energy integration makes the X-ray results sensitive to phonon dispersion effects. The results in Ref. 3 suggest a small dispersion for the lowest Peierls active phonon which we model by $\Omega_1(q_z) \approx \Omega_{1,q_0}(1+0.7|cq_z-\pi|^2)$ for $|cq_z-\pi| \ll 1$ with $\hbar\Omega_{1,q_0} \approx J$. While for a resolution of $\hbar\sigma_\omega = 0.05J$ the correlation length is basically independent of the dispersion (dash-dotted line in Fig. 10 (a)), the $\hbar\sigma_\omega = 0.5J$ data clearly are altered (dash-dotted line in Fig. 10 (b)).

(iv) The coupling constants $g_{\nu,\mathbf{q}}$ in Eq. (3) depend on the polarization vectors of the phonon modes.⁵ De-phazation effects suggest a suppression of $g_{\nu,\mathbf{q}}$ away from

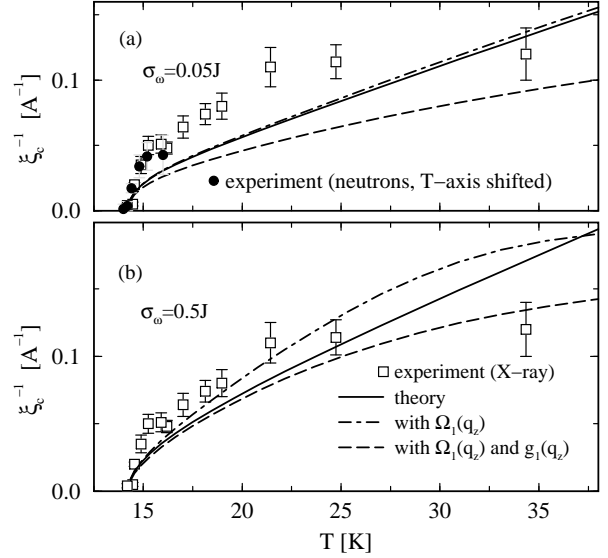


FIG. 10. Inverse correlation length along the magnetic chains from RPA compared with experimental data from Refs. 10 (squares) and 9 (circles). The lower resolution curves (a) are lower than those with larger σ modeling the X-ray experiment (b). The larger σ values are sensitive to the inclusion of the phonon dispersion into theory (dash-dotted lines). Including a Lorentzian shape of the spin-phonon coupling constants as a function of (q) leads to a saturation of $1/\xi$ at lower values (dashed lines).

\mathbf{q}_0 . We model this suppression in the normal coordinate propagator Eq. (7) by a Lorentzian along q_z

$$g_{\nu,\mathbf{q}}g_{\nu,-\mathbf{q}} \approx \frac{1 - \cos(q_z c)}{2} \frac{(c/\kappa)^2}{(c/\kappa)^2 + (q_z c - \pi)^2} |g_{\nu,\mathbf{q}_0}|^2. \quad (54)$$

The full and dash-dotted curves in Fig. 10 are obtained in the limit $c/\kappa \rightarrow \infty$. Setting $c/\kappa = 0.5$ yields the dashed curves in Fig. 10 (a) and (b). The saturation of the correlation length at higher temperatures suggests a value of $c/\kappa < 0.5$ for CuGeO_3 .

(v) Close to the phase transition neither the phonon dispersion nor the coupling constant's q_z dependence are important. The RPA results yield $\xi_c \sim (T - T_{\text{SP}})^{0.5}$ in agreement with detailed X-ray investigations by Harris *et al.*⁴³

(vi) The curves obtained for $J_2 = 0$ (not shown) lie about 30% below those for $J_2/J = 0.24$ (Fig. 10) suggesting that $\alpha = J_2/J \geq 0.24$ for CuGeO_3 .^{5,36}

The overall agreement of the description of the experimental data on the quasi-elastic scattering in CuGeO_3 is quite satisfactory. This suggests that indeed it is the precursor of the magneto-elastic mode discussed in the previous section.

IV. REAL SPACE INTERPRETATION

An open question is the appropriate real-space interpretation of the quasi-elastic scattering, especially in the central peak regime. To obtain a qualitative picture we consider the effective action in RPA as it was derived for example in Ref. 13. We limit ourselves here to a single phonon mode and only consider the physics within a chain of magnetic Cu ions. The action then reads in the static limit

$$\mathcal{S}_{\text{RPA}} = \beta \sum_{q_z} \hbar \Omega_{q_z} |\phi_{q_z}|^2 + \beta \sum_{q_z} \frac{g_{q_z} g_{-q_z}}{2} \chi_{\text{CF}}(-q_z, 0) |\phi_{-q_z}^* + \phi_{q_z}|^2. \quad (55)$$

The phonon fields ϕ_{q_z} and $\phi_{q_z}^*$ are directly related to the Bose operators b_q and b_q^\dagger in the minimal model discussed in Sec. II.

The first term of Eq. (55) simply corresponds to the phonon Hamiltonian H_p in Eq. (12) of the minimal model. The second term of Eq. (55) is the relevant correction term. Within the approximations made and neglecting the momentum dependence of the polarization vector the coupling constants are given by

$$\frac{g_{q_z} g_{-q_z}}{2} = [1 - \cos(q_z c)] (g_{\text{Cu}}^z)^2 \frac{\hbar}{2\Omega_{q_z} m_{\text{Cu}}}, \quad (56)$$

g_{Cu}^z is the change of J with the Cu elongation, and m_{Cu} is the Cu mass.⁵

The appropriate transformation of the reciprocal-space fields $\phi_{q_z}^*$ to real-space elongation fields u_{l_z} is

$$\phi_{-q_z}^* + \phi_{q_z} = \sqrt{\frac{2\Omega_{q_z} m_{\text{Cu}}}{\hbar L}} \sum_{l_z} e^{-iq_z c l_z} u_{l_z}, \quad (57)$$

the conjugated momenta are given by

$$\phi_{-q_z}^* - \phi_{q_z} = \frac{1}{i} \sqrt{\frac{1}{2\hbar\Omega_{q_z} m_{\text{Cu}} L}} \sum_{l_z} e^{-iq_z c l_z} p_{l_z}. \quad (58)$$

The q_z dependence of the dimer-dimer correlation function $\chi_{\text{CF}}(q_z, 0)$ is satisfactorily approximated by a Lorentzian

$$\chi_{\text{CF}}(q_z, 0) \approx \frac{-\chi_0(\frac{k_B T}{J})}{k_B T} \frac{(c/\xi_D)^2}{(c/\xi_D)^2 + (q_z c - \pi)^2}. \quad (59)$$

The dimer length scale was defined as

$$\xi_D^{-1} = 0.53 \frac{2\pi}{\hbar v_s} k_B T. \quad (60)$$

Introducing the dispersion as given in Eq. (11) and applying Eqs. (56) through (60) to Eq. (55) the action becomes

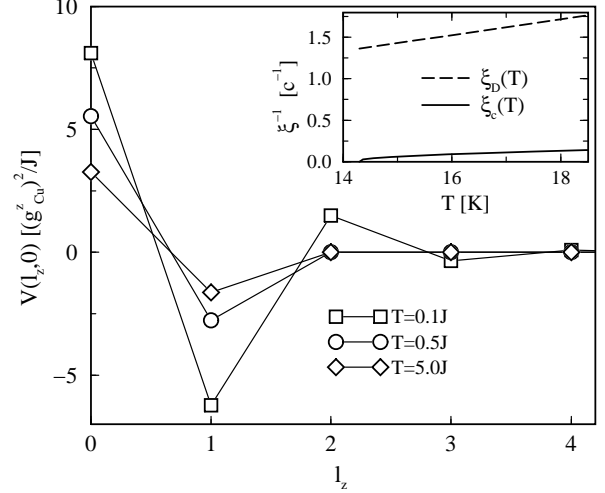


FIG. 11. Spin-phonon coupling induced dimerization potential as given in Eqs. (62) and (63) for different temperatures and $J_2/J = 0.24$. The inset shows the inverse dimer correlation length as in Eq. (60), dashed line, in comparison with the spin-Peierls correlation length, full line identical to the full line in Fig. 10 (a).

$$\mathcal{S}_{\text{RPA}} \approx \beta \sum_{l_z} \frac{p_{l_z}^2}{2m_{\text{Cu}}} + \frac{\Omega_{\pi}^2 m_{\text{Cu}}}{8} (u_l - u_{l+1})^2 - \beta \sum_{l_z, l'_z} V(l_z, l'_z) u_{l_z} u_{l'_z}. \quad (61)$$

The dimer-dimer correlation induced potential

$$V(l_z, l'_z) = V_0 \left[\delta_{l_z=l'_z} + \frac{\delta_{l_z \neq l'_z}}{2} (-1)^{|l_z - l'_z|} \times e^{-\frac{c|l_z - l'_z|}{\xi_D}} (1 + \cosh \frac{c}{\xi_D}) \right] \quad (62)$$

with amplitude

$$V_0 = (g_{\text{Cu}}^z)^2 \frac{1.06\pi c}{\hbar v_s} \chi_0 \left(\frac{k_B T}{J} \right) \quad (63)$$

is alternating in space and decaying on the length scale of $\xi_D \sim T^{-1}$. The amplitude of the potential is determined by $\chi_0(k_B T/J)$ of which the temperature dependence is shown in Ref. 42. It is enhanced for $T < J/k_B$ and appears to vanish for $T \rightarrow 0$ for $J_2 = 0$ while it might even diverge for $J_2/J \geq 0.241$. The potential $V(l_z, 0)$ is plotted for different temperature for $J_2/J = 0.24$ in Fig. 11. Note that $V(l_z, l'_z)$ is translational invariant.

This potential enhances local dimerization on the length scale ξ_D . It is crucial to distinguish $\xi_c \neq \xi_D$ (see inset of Fig. 11). The correlation length of the spin-Peierls transition ξ_c describes fluctuations to be associated with the coherent three-dimensional ordering of the local dimerized areas of scale ξ_D . This coherent dimer-ordering in CuGeO_3 has been described very successfully via effective Ising based mean-field models.^{13,6,7,44}

In this sense the spin-Peierls transition in CuGeO_3 can be considered as a order-disorder transition where the objects that order are only induced by the spin system as the temperature is lowered substantially below J/k_B . The coherent ordering leads to tricritical behavior⁶ with a tricritical to mean-field crossover temperature of $T_{\text{CR}} - T_{\text{SP}} \approx 0.1$ K coinciding with the appearance of large length scale fluctuations.¹¹

A straightforward determination of the magnetic dimer correlation length in Eq. (60) with the parameters for CuGeO_3 as discussed above yields $\xi_D(T_{\text{SP}}) \approx 0.7c$. Considering the momentum dependence of the coupling constants as discussed in Eq. (54) rescales the magnetic dimer correlation length roughly as $\xi_D \approx \sqrt{\xi_D^2 + \kappa^2}$. For $c/\kappa = 0.5$ one has $\xi_D(T_{\text{SP}}) \approx 2c$ which then is basically temperature independent. The order of magnitude is reasonable.

Note that this real-space interpretation is consistent with the pre-transitional pseudo-gap behaviour discussed in the context of Peierls transitions.⁴⁵⁻⁴⁷

V. CONCLUSIONS

We discussed in detail magneto-elastic excitations in systems of phonons coupled to spin chains within the random phase approximation. The XY model allowed for an exact determination of the temperature dependence of the poles of the dynamical structure factor in the disordered as well as in the dimerized phase in both the soft phonon and the central peak regime. The model of frustrated Heisenberg chains coupled to phonons applied to the spin-Peierls system CuGeO_3 correctly describes the details of the quasi-elastic scattering such as its frequency dependence, momentum space dependence, and the extracted correlation lengths. The importance of the experimental energy resolution is emphasized.

The quasi-elastic scattering can be interpreted as the precursor of a new magneto-elastic excitation in the dynamical phonon structure factor for $T < T_{\text{SP}}$ which increasingly splits off from the scattering continuum as the temperature is lowered. In alternating Heisenberg chains relevant for CuGeO_3 this leads to a renormalization of the singlet bound state by about 10 %. In alternating XY chains the position and temperature dependence of this excitation can be calculated explicitly and compares favorably with the 30 cm^{-1} mode found in inelastic light scattering experiments, thus yielding a qualitatively modified explanation of this signal.

The real-space interpretation of a spin-phonon induced alternating elastic potential supports the applicability of Ising-like approaches to the spin Peierls transition. The spin-phonon induced alternating elastic potential driving the transition underlines the mixed magneto-elastic character of quasi-elastic scattering.

VI. ACKNOWLEDGMENTS

We are indebted to M. Braden for furnishing the neutron scattering data files and instructive discussions. We thank P. Lemmens for providing ILS data for the 30 cm^{-1} mode and discussions. We thank A. P. Kampf, A. Weiße, and A. Zheludev for stimulating discussions. The work performed in Bayreuth and in Wuppertal was supported by DFG program “Schwerpunkt 1073”, the work at BNL was supported by DOE contract number DE-AC02-98CH10886.

-
- ¹ M. C. Cross and D. S. Fisher, Phys. Rev. B **19**, 402 (1979).
 - ² C. Gros and R. Werner, Phys. Rev. B **58**, R14677 (1998).
 - ³ M. Braden *et al.*, Phys. Rev. Lett. **80**, 3634 (1998).
 - ⁴ A. Klümper, R. Raupach, and F. Schöfeld, Phys. Rev. B **59**, 3612 (1999).
 - ⁵ R. Werner, C. Gros, and M. Braden, Phys. Rev. B **59**, 14356 (1999).
 - ⁶ R. J. Birgeneau, V. Kiryukhin, and Y. J. Wang, Phys. Rev. B **60**, 14816 (1999).
 - ⁷ S. M. Bhattacharjee, T. Nattermann, and C. Ronnewinkel, Phys. Rev. B **58**, 2658 (1998).
 - ⁸ M. Braden, *Quantitative Analyse einer magnetoelastischen Kopplung am Beispiel von CuGeO₃* (Habilitation, Aachen, 1999).
 - ⁹ K. Hirota *et al.*, Phys. Rev. B **52**, 15412 (1995).
 - ¹⁰ J. P. Schoeffel, J. P. Pouget, G. Dhalenne, and A. Revcolevschi, Phys. Rev. B **53**, 14971 (1996).
 - ¹¹ Y. J. Wang *et al.*, preprint, cond-mat/0004363 (2000).
 - ¹² R. Werner, preprint, cond-mat/0006168 (2000).
 - ¹³ R. Werner, *The spin-Peierls transition in CuGeO₃* (Ph.D. thesis, Dortmund, 1999), <http://eldorado.uni-dortmund.de:8080/FB2/ls8/forschung/1999/werner>.
 - ¹⁴ M. Karbach and G. Müller, Comp. in Phys. **11**, 36 (1997), M. Karbach and G. Müller, Comp. in Phys. **12**, 565 (1998), M. Karbach, K. Hu, and G. Müller, to appear in Comp. in Phys. (2000).
 - ¹⁵ K. Fabricius, U. Löw, and J. Stolze, Phys. Rev. B **55**, 5833 (1997).
 - ¹⁶ E. F. Fradkin, *Field Theories of Condensed Matter Systems* (Addison-Wesley, New York, 1991).
 - ¹⁷ Y. Yu, G. Müller, and V. Viswanath, Phys. Rev. B **54**, 9242 (1996).
 - ¹⁸ L. G. Caron and S. Moukouri, Phys. Rev. Lett. **76**, 4050 (1996).
 - ¹⁹ J. W. Bray, L. V. Interrante, I. S. Jacobs, and J. C. Bonner, in *Extended Linear Chain Compounds*, edited by J. S. Miller (Plenum, New York, 1983), Vol. 3, p. 353, as pointed out by these authors an Ising or classical antiferromagnetic Heisenberg chain cannot show the spin-Peierls effect. This is because there is a gap in the magnetic excitation spectrum for the Ising case and no ground-state degeneracy for the Heisenberg case, i.e., in both cases it is energetically not favorable for the 1D chain to dimerize.

- ²⁰ The use of one-dimensional phonons is justified, because the RPA approach does only contain summations over different phonon branches, but not over different values of \mathbf{q} .
- ²¹ G. D. Mahan, *Many-Particle Physics* (Plenum Press, New York, 1981).
- ²² R. A. T. Lima and C. Tsallis, *Solid State Commun.* **40**, 155 (1981).
- ²³ G. Beni and P. Pincus, *J. Chem. Phys.* **57**, 72 (1972).
- ²⁴ M. Holicki, *Zur Natur des spin-Peierls-Übergangs* (Diploma thesis, Bayreuth, 2000).
- ²⁵ G. Wellein, A. P. Kampf, and H. Fehske, *Phys. Rev. Lett.* **81**, 3956 (1998).
- ²⁶ S. Engelsberg and J. R. Schrieffer, *Phys. Rev.* **131**, 993 (1963).
- ²⁷ G. Els *et al.*, *Phys. Rev. Lett.* **79**, 5138 (1997).
- ²⁸ P. Lemmens, private communication.
- ²⁹ A. Weiße, G. Wellein, and H. Fehske, *Phys. Rev. B* **60**, 6566 (1999).
- ³⁰ G. S. Uhrig and H. J. Schulz, *PRB* **54**, R9624 (1996).
- ³¹ F. H. L. Essler, A. M. Tsvelik, and G. Delfino, *Phys. Rev. B* **56**, 11001 (1997).
- ³² M. Hase, I. Terasaki, and K. Uchinokura, *Phys. Rev. Lett.* **70**, 3651 (1993).
- ³³ G. Castilla, S. Chakravarty, and V. J. Emery, *Phys. Rev. Lett.* **75**, 1823 (1995).
- ³⁴ J. Riera and A. Dobry, *Phys. Rev. B* **51**, 16098 (1995).
- ³⁵ K. Fabricius *et al.*, *Phys. Rev. B* **57**, 1102 (1998).
- ³⁶ W. Brenig, *Phys. Rev. B* **56**, 14441 (1997).
- ³⁷ A. Fledderjohann and C. Gros, *Europhys. Lett.* **37**, 189 (1997).
- ³⁸ A. M. Tsvelik, *Quantum field theory in condensed matter physics* (Cambridge University Press, Cambridge, 1995).
- ³⁹ H. J. Schulz, *Phys. Rev. B* **34**, 6372 (1986).
- ⁴⁰ N. M. Bogoliubov and V. E. Korepin, *Int. J. Mod. Phys. B* **3**, 427 (1981).
- ⁴¹ R. Chitra *et al.*, *Phys. Rev. B* **52**, 6581 (1995).
- ⁴² R. Raupach, A. Klümper, and F. Schönfeld, preprint, cond-mat/9908407 (1999).
- ⁴³ Q. J. Harris *et al.*, *Phys. Rev. B* **52**, 15420 (1995).
- ⁴⁴ R. Werner and C. Gros, *Phys. Rev. B* **57**, 2897 (1998).
- ⁴⁵ P. A. Lee, T. M. Rice, and P. W. Anderson, *Phys. Rev. Lett.* **31**, 462 (1973).
- ⁴⁶ R. H. McKenzie, *Phys. Rev. B* **51**, 6249 (1995).
- ⁴⁷ R. H. McKenzie, *Phys. Rev. B* **52**, 16428 (1995).